Editors' Suggestion | Featured in Physics

Oscillations of Drops with Mobile Contact Lines on the International Space Station: Elucidation of Terrestrial Inertial Droplet Spreading

J. McCraney,[1] V. Kern,[1] J. B. Bostwick,[2] S. Daniel,[1] and P. H. Steen[1]
[1]Robert Frederick Smith School of Chemical and Biomolecular Engineering, Cornell University, Ithaca, New York 14853, USA
[2]Department of Mechanical Engineering, Clemson University, Clemson, South Carolina 29634, USA

(Received 15 February 2022; accepted 11 July 2022; published 16 August 2022)

We analyze shape oscillations of sessile water drops with fully mobile contact lines (CL) aboard the International Space Station. The unique microgravity environment enables the study of centimeter-sized droplets with associated inertial-capillary motions. Plane-normal substrate vibrations induce resonance behaviors quantified by frequency scans from which the natural frequencies and mode shapes are identified for nine different hydrophobic surfaces. Experimental observations agree well with, and validate, a recent spectral prediction of mobile CL sessile drop oscillations. The experimental findings help elucidate terrestrial droplet inertial spreading, a poorly understood phenomenon pervasive in many processes.

DOI: 10.1103/PhysRevLett.129.084501

Droplet motions on substrates are intrinsic to numerous industrial processes and technologies, such as step and imprint lithography in semiconductor manufacturing [1], additive manufacturing [2], spray cooling [3], drop impacts [4–6], and the assembly of autonomous fluidic machines [7]. The sessile drop is the canonical problem upon which the aforementioned applications are based and highlights the inherent multiphysics in the inertial wetting phenomena. In classifying the dynamics, drops can move on a contacting surface with relative ease (free drops); others resist surface movement and spread or recede slowly (partially free drops), while others do not move on the surface (pinned drops). This range of behaviors can be quantified by the mobility Λ of the three-phase contact lines (CL) which is unique to the particular liquid-solid-gas system and flow conditions. On Earth, drop CL displacements are on the order of 50 μm and of similar scale to the surface roughness, making experimental realization of fully mobile CLs nearly impossible, with the closest exception being slippery liquid-infused porous surfaces [8–10]. However, in microgravity it is possible to overcome such defects to generate fully mobile CL conditions $\Lambda = 0$. In this Letter, we report an experimental study from the International Space Station (ISS) of sessile drop oscillations with fully mobile CLs, enabled by flow conditions realized in microgravity. This critical insight enables precise predictions of CL spreading, pervasive throughout terrestrial processes, but which has largely eluded experimental analysis.

A sessile drop in equilibrium is defined by the base radius a and static contact angle (CA) α, as shown in Fig. 1(a). Shape oscillations can be excited by plane-normal vibrations of the substrate, which induce CL motions with physics governed by a constitutive relationship relating CA deviations $\Delta\alpha$ to the contact-line speed u_{CL} [cf. Fig. 1(b)], which upon linearization about $u_{\mathrm{CL}} = 0$ yields the Davis-Hocking [11,12] dynamic contact-line law

$$\Delta\alpha = \Lambda u_{\mathrm{CL}}. \tag{1}$$

Here Λ is the contact-line mobility, sometimes referred to as a homotopy parameter such that $\Lambda \in [0, \infty]$ with limiting cases of (i) $\Lambda = 0$ a fully mobile CL (fixed CA) and (ii) $\Lambda = \infty$ pinned CL. Intermediate cases $\Lambda \neq 0, \infty$ exhibit finite CL mobility and can induce dissipation, even in inviscid fluids. Bostwick and Steen [13] computed the frequency spectrum from an operator equation,

$$\hat{\Omega}^2 M[y] = K[y], \tag{2}$$

showing how the scaled drop frequency $\hat{\Omega} \equiv 2\pi\Omega\sqrt{\sigma/\rho a^3}$ depends upon the wetting parameters $\hat{\Omega}_{[k,l]}(\alpha, \Lambda)$ where ρ and σ are density and surface tension. The corresponding mode shapes $y_{[k,l]}$ are defined by the mode number pair $[k, l]$ inherited from the spherical harmonics [14], as shown in Fig. 1(c). Steen *et al.* [15] have recast the problem using a symmetry-breaking perspective and shown how the sessile drop spectrum can be organized into a "periodic table of droplet motions," making an analogy with the periodic table of chemical elements. Theoretical predictions include splitting of the Rayleigh drop degeneracy [16], spectral reordering, and mode mixing, all of which have been experimentally verified by Chang *et al.* [17,18], who have observed the first 37 resonance modes for pinned CL conditions $\Lambda = \infty$. Enforcing pinned CL conditions experimentally can be achieved either through (i) mechanical pinning of the CL by a finite-sized surface defect or

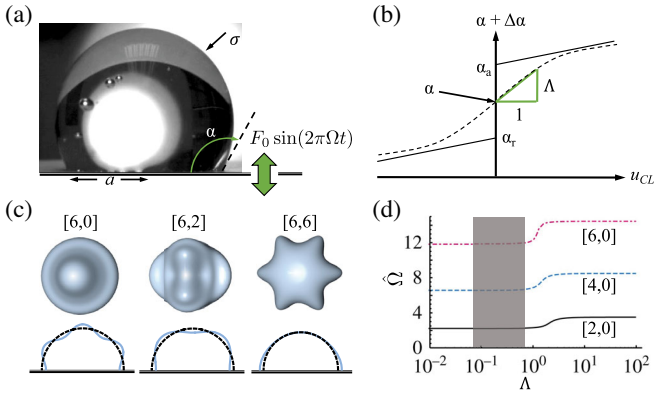

FIG. 1. (a) Definition sketch of driven sessile drop with base radius a and contact-angle α whose contact line obeys (b) a dynamic contact-line law which relates α to the contact-line speed u_{CL} through the contact-line mobility parameter Λ and advancing α_a and receding α_r contact angles. (c) Under resonant conditions, the drop will oscillate with characteristic frequency Ω and shape defined by the mode number pair $[k, l]$ classified using spherical harmonic terminology into zonal [6,0], tesseral [6,2], and sectoral [6,6] shapes. (d) Theoretical prediction of the scaled oscillation frequency $\hat{\Omega}$ for the first three axisymmetric modes against mobility Λ for $\alpha = 105°$ illustrates the limiting cases of the fully mobile $\Lambda = 0$ and pinned $\Lambda = \infty$ contact line, with the shadowed region denoting the experimental parameter range.

(ii) using high CA hysteresis surfaces, which effectively immobilizes the CL for small interface disturbances [19,20]. Pinned CLs are common in drop oscillation experiments [21–23]. In contrast, the observation of fully mobile contact-line motions $\Lambda = 0$ has been elusive, with the notable exception of the recent study by Xia and Steen [24] that was focused on CL motions with finite mobility $\Lambda \neq 0, \infty$.

Our experimental study fills this gap by leveraging the unique microgravity environment aboard the ISS. The advantage of microgravity is the magnification of the capillary length $\ell = \sqrt{\sigma/\rho g}$ and time $t_c = \sqrt{\rho a^3/\sigma}$ scales. On Earth $\ell = 3$ mm, but since $\ell \sim 1/\sqrt{g}$, the microgravity acceleration $g \sim 10^{-6}$ m/s^2 implies $\ell \sim 1$ m, allowing for experimentation with centimeter-sized drops, 10 times larger than those typically used in terrestrial conditions, with corresponding 30-fold amplification in timescale. The ISS is enabling, allowing for accurate spatial and temporal resolution of the CL dynamics, particularly for hydrophobic surfaces, where inertial-capillary motion is favored by liquids that do not strongly wet the solid [24]. Most importantly, the CL displacements associated with these large length scales are sufficient to overcome the micrometer-sized defects associated with surface roughness that can induce CL pinning and stick-slip behaviors. Figure 2 shows the time evolution of a mobile drop oscillating in the [2, 0] mode, where comparing time 0 s to 0.31 s illustrates large CL displacements. Of course it is not possible to have a perfect $\Lambda = 0$ surface; however, for sufficiently small Λ,

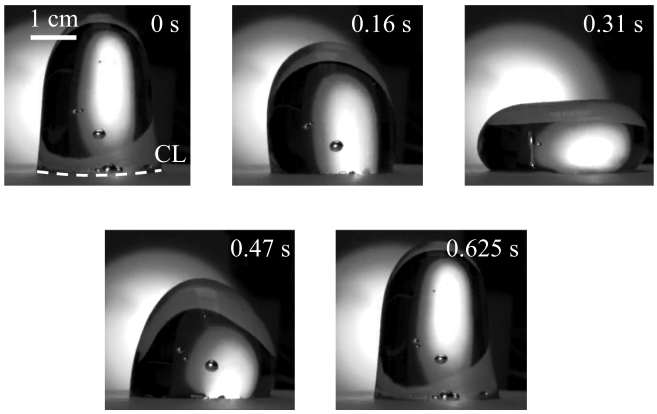

FIG. 2. Droplet driven at 1.6 Hz oscillating in the [2,0] mode on substrate F_7 exhibits a freely moving contact line.

drop resonance $\hat{\Omega}$ is nearly identical to the fully mobile $\Lambda = 0$ case, as evidenced by the horizontal regions shown in Fig. 1(d) for $0 \leq \Lambda \lesssim 1$, which plots $\hat{\Omega}$ against Λ for a typical experiment. We have measured Λ using the technique of Xia and Steen [25] for all substrates used in our experiments, finding that Λ falls within the shadowed region of Fig. 1(d). Given that our experiments fall within the lower frequency plateau region for all modes, we are comfortable in comparing our experimental results with the $\Lambda = 0$ theoretical predictions.

Experiment.—Experiments were conducted aboard the ISS Observation and Analysis of Smectic Islands in Space (OASIS) system within the OASIS bubble chamber, as schematically shown in Fig. 3. A 10 mL water drop with density $\rho = 1$ g/mL, surface tension $\sigma = 72$ mN/m, and viscosity $\mu = 10^{-3}$ Pa s is deposited onto a partially wetting substrate via a syringe. Nine substrates were prepared with a wide range of wetting properties $\alpha, \alpha_a, \alpha_r, a$, given in Table I, where α and a were geometrically measured by fitting a circle to the drop shape at rest. These substrates were designed to be low friction and produce freely moving contact lines, with the exception of substrate P_1 which was fabricated with a circular indentation of radius 1.5 cm to mechanically "pin" the contact line. The substrate is oscillated in the normal direction by a PASCO Scientific SF-9324 mechanical wave driver with prescribed amplitude range $F_0 = 0.6$–1.7 mm and frequency f_d controlled via a PASCO WA-9867 sine wave generator, generating accelerations from 0.0002 to 0.24 g. Motions are captured at

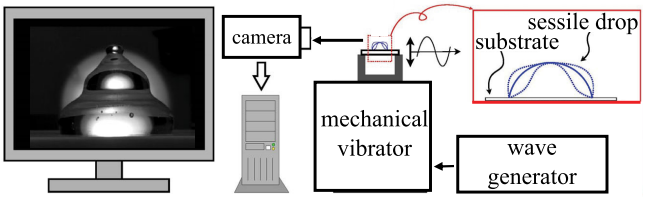

FIG. 3. Experimental schematic.

TABLE I. Substrate identification table with wetting properties $\alpha, \alpha_a, \alpha_r$. Substrates labeled F_x denote free drop conditions, whereas substrate P_1 is fabricated with a 1.5 cm radius pinning site to produce pinned drop conditions.

ID	Substrate	Modification	$\alpha(^\circ)$	$\alpha_a(^\circ)$	$\alpha_r(^\circ)$	a(cm)
F_1	Silicon	PDMS	106	108	99	1.65
F_2	Silicon	Fluorosilane	114	121	90	1.59
F_3	Glass	PDMS	102	106	96	1.66
F_4	Glass	Fluorosilane	112	122	84	1.60
F_5	Teflon	Unsanded	115	116	77	1.57
F_6	Teflon	320 grit sanded	130	155	100	1.42
F_7	Teflon	240 grit sanded	143	163	62	1.23
F_8	Teflon	120 grit sanded	128	148	59	1.44
P_1	Silicon	Fluorosilane	135	N/A	N/A	1.35

148 fps via a PixeLink M4-CYL high-speed camera backlit via LED lighting.

A frequency scan was performed for each substrate for a range of driving frequencies $f_d = 1$–10 Hz with a frequency interval of 0.2 Hz. Here we waited 5 sec before proceeding to the next successive frequency. Near resonance, the drop oscillates with fundamental mode shape $[k, l]$ described by theory [13]. Modal identification is achieved by comparing side-view perspective droplet shapes to theoretical predictions using two techniques. The first has been utilized in terrestrial-based drop vibration experiments [18,23], where the magnitude of the interfacial disturbance from equilibrium is measured and the resonance is defined by the largest such deflection. This technique is illustrated in the top row of Fig. 4, where a series of drop images are overlaid at the prescribed driving frequency. Here it is clear the maximal deflection for the [4,0] mode occurs at 4.0 Hz. This techniques works well whenever the resonance frequency for that particular mode is isolated. However, in some cases, two or more modes $[k, l]$ may have nearly identical resonance frequencies. This is shown in the bottom row of Fig. 4. Here the asymmetric [5,1] mode only appears at 6.2 Hz and lies in between an axisymmetric mode at slightly lower (6.0 Hz) and higher (6.4 Hz) frequencies. For this second technique, once a resonant mode shape is identified via comparison to the predicted shape, the oscillation frequency f is determined via a fast Fourier transform with respect to time. Here in-house developed tracking algorithms were utilized to reduce image noise and to adequately resolve both the liquid or gas interface and contact-line region. We note that all observed motions are harmonic, i.e., the oscillation frequency is equal to the driving frequency $f = f_d$, which is distinguished from terrestrial-based experimental studies of pinned contact-line sessile drop vibrations, some of which exhibit a subharmonic response, $f = f_d/2$.

Results.—Figure 5 presents a catalogue of the experimentally observed modes $[k, l]$, as described by the classification scheme of Steen *et al.* [15]. We note the

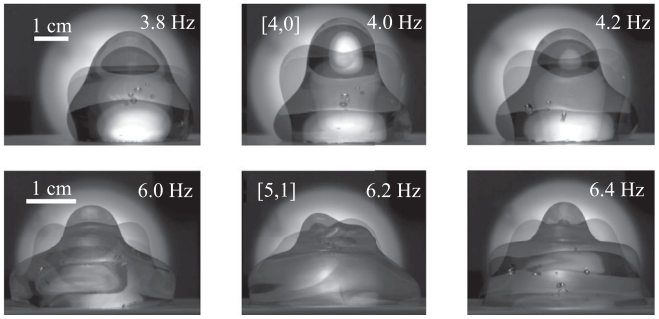

FIG. 4. Resonance identification from overlaid images for sequential driving frequencies. Top row: the [4, 0] mode persists over the entire frequency range exhibiting maximal extension at resonance $f_d = 4.0$ Hz for substrate F_4. Bottom row: the [5, 1] mode exists only in a small frequency window at $f_d = 6.2$ Hz that lies between axisymmetric shapes for substrate F_5.

zonal modes [2,0], [4,0], [6,0] were observed on every substrate tested, whereas the tesseral modes [3,1], [5,1], [6,2], [6,4] were not. Several modes were undetected altogether, including sectoral modes $[2, 2], [3, 3], \ldots, [k, k]$, which we attribute to the discrete 0.2 Hz interval of the frequency scan. More specifically, if the resonance frequency for that particular mode lies within the frequency interval and has a small bandwidth then it is possible that this mode was skipped during the frequency scan. In addition, whenever two modes have nearly the same resonance frequency modal competition can occur, as described by Chang *et al.* [18], and in this case the lower energy mode saturates the droplet response making the higher energy mode nearly undiscoverable except in a small frequency range. Lastly, we note that poor lighting and droplet positioning could have played a role in modal discovery, as well as the practicalities of performing experiments aboard the ISS in a microgravity environment with corresponding time constraints. Despite these challenges, our experiments yielded a large dataset over a range of hydrophobic-to-superhydrophobic wetting conditions $102^\circ < \alpha < 143^\circ$ with freely moving contact lines.

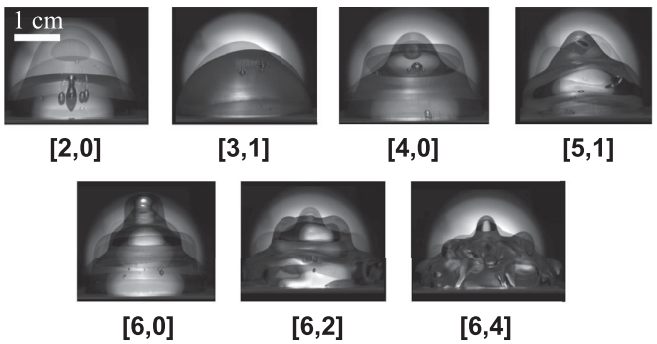

FIG. 5. Experimentally-observed modes $[k, l]$ overlaid throughout an oscillation cycle.

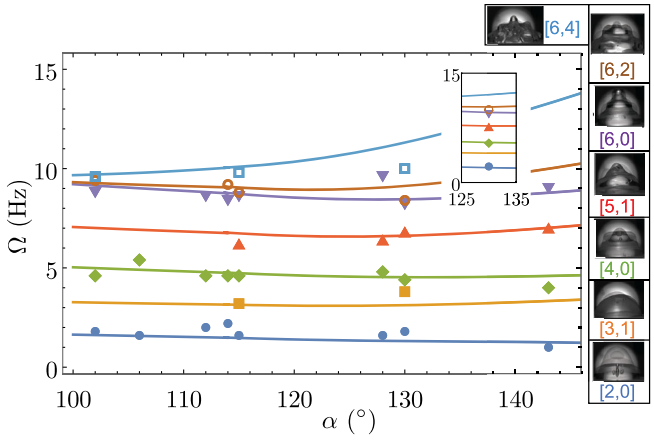

FIG. 6. Frequency (Hz) against static contact angle $\alpha(^\circ)$ contrasting experiment (symbols) with theoretical predictions with free contact lines $\Lambda = 0$ (solid lines) for modes $[k, l]$ on substrates $F_1 - F_8$. Inset: a plot of frequency Ω for substrate P_1 for pinned drops. Experimental error ± 0.2 Hz is defined by the symbol size.

Figure 6 plots the resonance frequency against the contact angle α contrasting experimental observations (symbols) with theoretical predictions (solid lines) from Bostwick and Steen [13] for free contact lines $\Lambda = 0$. The figure inset corresponds to substrate P_1 with pinned contact line $\Lambda = \infty$. We note the excellent agreement between experiment and theory, especially for the zonal modes $[k, 0]$ over a large range of α. The higher energy modes [6,2], [6,4] tend to undershoot theoretical predictions as α deviates further from hemispherical $\alpha = 90^\circ$, which is consistent with other studies [18]. The experimental frequencies agree with theory within 9%, and excluding the [2, 0] mode, agree within 4.3% at maximum with most observations falling within 1%. Given the potential sources of error described above, this excellent agreement suggests (1) the experiments indeed produce drops with freely moving CLs (corroborating independent image analysis) and (2) the model captures the essential physics of oscillating sessile drops with freely moving CLs.

It is interesting to contrast the results for substrates F_6 and P_1, given that they have similar static contact angle $\alpha = 130^\circ$–135° but dramatically different contact-line dynamics. Substrate F_6 produces fully mobile $\Lambda = 0$ contact lines, whereas substrate P_1 produces fully immobile $\Lambda = \infty$ contact lines, thus encompassing both extremes of the more general contact-line dynamics $\Lambda \neq 0, \infty$. Table II shows that the resonance frequencies for the pinned drop (substrate P_1) are always larger than that for the free drop (substrate F_6) consistent with our mathematical understanding that a pinned contact-line boundary condition tends to "constrain" the drop more than the free contact-line boundary condition from an energy variational sense [26]. Our experimental results verify this understanding of the contact-line physics.

TABLE II. Resonant frequencies [Hz] contrasting free F_6 $\alpha = 130^\circ$ and pinned P_1 $\alpha = 135^\circ$ CLs.

Mode	[2,0]	[3,1]	[4,0]	[5,1]	[6,0]	[6,2]	[6,4]
F_6 (Hz)	1.8	3.8	4.4	6.8	8.2	8.4	10
P_1 (Hz)	2.2	⋯	5.4	7.6	9.4	10	⋯

Lastly, we note all of our experiments produced drop resonances with a harmonic response, in contrast to terrestrial-based experimental studies of pinned drops [17,18], which exhibited more complicated dynamics; the zonal modes $[k, 0]$ responded harmonically but the sectoral $[k, k]$ and tesseral $[k, l \neq k]$ modes responded subharmonically. Typically, a subharmonic droplet response is associated with the onset of Faraday waves with corresponding onset acceleration, i.e., the drop interface remains undeformed until a critical (and finite) forcing acceleration is reached upon which the wave is formed on the interface [27]. This is commonly referred to as Faraday wave onset. In contrast, a harmonic droplet response typically occurs for all values of the driving acceleration as axisymmetric traveling waves are excited from the contact line and constructively or destructively interfere with one another at the drop apex creating a standing wave pattern in the form of a zonal mode. Given our observations that all modes respond harmonically, it is reasonable to conclude the forcing amplitudes used in our experiments are smaller than required for Faraday wave onset. This is most likely related to the (i) low drop weights inherent in microgravity and (ii) comparably small capillary pressures, which scale inversely with the drop radius r^{-1}, that must be overcome to excite shape oscillations.

Discussion.—We have reported the results of an experimental study of oscillating sessile drops on hydrophobic surfaces over a wide range of wetting properties. The experiments were conducted in the microgravity environment aboard the ISS enabling fully mobile contact-line dynamics with corresponding physics, which have heretofore been unrealized in terrestrial-based experiments. The large capillary lengths possible in microgravity permitted the use of centimeter-scale drops with CL deformation able to overcome the typical micrometer-size surface defects which are known to cause contact-line pinning in millimeter-size water drops. Resonance frequencies were measured for seven mode shapes and compared with theoretical predictions, showing good agreement, thus suggesting our model adequately captures the physics of mobile contact lines for oscillating drops.

Fully mobile contact-line dynamics are a limiting case of the more general, and often increasingly complex, area of dynamic wetting, which can yield motions such as stick slip [28] and air entrainment, among others [29]. The Davis-Hocking model [Eq. (1)] is often invoked in theoretical studies involving contact-line motions so much that the question has been recently asked "is the contact-line

mobility Λ a material parameter" that can be measured [24,30]. This is an open question, particularly for capillary-ballistic motions characterized by a high Reynolds number Re and moderate Weber number We, $\mathrm{Re} > \sqrt{\mathrm{We}}$, defining the inertial spreading regime. Our study helps to answer this question by producing experimental results for the most sought-after extreme $\Lambda = 0$ (fully mobile CL) which when combined with prior results for the other extreme $\Lambda = \infty$ (pin CL) will aid in designing future studies to explore the finite Λ regime.

Recent advances in manufacturing have led to the fabrication of "designer surfaces" with controllable wetting properties through combinations of surface chemistry, roughness, and microstructure [31,32]. The ever shrinking length scale of surface defects in these fabrication processes will inevitably lead to the realization of drop motions with fully mobile CLs under terrestrial conditions [33,34]. Numerous microgravity technologies involve free CL motions including wickless heat pipes for thermal management [35], fuel management devices [36], and the more general handling of fluids via capillary drainage [37,38], some of which are mission critical. For example, in the NEAR anomaly spreading of hydrophobic fuels, e.g., a "green" hydroxyl ammonium nitrate fuel and oxidizer blend AF-M315E [39], during dynamic flight maneuvers sent the spacecraft into safety mode, thereby losing communication for approximately 27 hours and delaying the intended mission by over a year [40]. Given the criticality of these current and future areas of technology, our canonical study of sessile drop motions with free CLs is both essential and timely to the field of inertial wetting dynamics.

Special thanks to NASA astronauts Kathleen Rubins and Michael Hopkins for their patience and insight in performing the experiments. Thanks to Jonathan Ludwicki for experimental design assistance. The authors acknowledge the role of Professor P. H. Steen in leading this research, and note his passing before the time of publication. We are honored to be able to continue this work and bring it to the field. We gratefully acknowledge support from NSF Grants No. 1530522, No. 1637960, and No. 1935590 and NASA Grant No. 80NSSC19K0406.

[1] E. A. Costner, M. W. Lin, W. L. Jen, and C. G. Willson, Annu. Rev. Mater. Res. **39**, 155 (2009).
[2] B. Derby, Engineering **1**, 113 (2015).
[3] J. Li, Y. Hou, Y. Liu, C. Hao, M. Li, M. K. Chaudhury, S. Yao, and Z. Wang, Nat. Phys. **12**, 606 (2016).
[4] S. T. Thoroddsen, M.-J. Thoraval, K. Takehara, and T. G. Etoh, Phys. Rev. Lett. **106**, 034501 (2011).
[5] G. Riboux and J. M. Gordillo, Phys. Rev. Lett. **113**, 024507 (2014).
[6] K. Cardin, S. Wang, O. Desjardins, and M. Weislogel, Phys. Rev. Fluids **6**, 014003 (2021).
[7] N. J. Cira, A. Benusiglio, and M. Prakash, Nature (London) **519**, 446 (2015).
[8] T.-S. Wong, S. H. Kang, S. K. Tang, E. J. Smythe, B. D. Hatton, A. Grinthal, and J. Aizenberg, Nature (London) **477**, 443 (2011).
[9] P. Juuti, J. Haapanen, C. Stenroos, H. Niemelä-Anttonen, J. Harra, H. Koivuluoto, H. Teisala, J. Lahti, M. Tuominen, J. Kuusipalo *et al.*, Appl. Phys. Lett. **110**, 161603 (2017).
[10] C. Zhang, S. Adera, J. Aizenberg, and Z. Chen, ACS Appl. Mater. Interfaces **13**, 15901 (2021).
[11] L. M. Hocking, J. Fluid Mech. **179**, 253 (1987).
[12] S. H. Davis, J. Fluid Mech. **98**, 225 (1980).
[13] J. B. Bostwick and P. H. Steen, J. Fluid Mech. **760**, 5 (2014).
[14] T. MacRobert, *Spherical Harmonics* (Pergamon, New York, NY, 1967).
[15] P. H. Steen, C. T. Chang, and J. B. Bostwick, Proc. Natl. Acad. Sci. U.S.A. **116**, 4849 (2019).
[16] L. Rayleigh, Proc. R. Soc. London **29**, 71 (1879).
[17] C.-T. Chang, J. B. Bostwick, P. H. Steen, and S. Daniel, Phys. Rev. E **88**, 023015 (2013).
[18] C.-T. Chang, J. Bostwick, S. Daniel, and P. Steen, J. Fluid Mech. **768**, 442 (2015).
[19] D. t Mannetje, S. Ghosh, R. Lagraauw, S. Otten, A. Pit, C. Berendsen, J. Zeegers, D. van den Ende, and F. Mugele, Nat. Commun. **5**, 3559 (2014).
[20] G. Fang, W. Li, X. Wang, and G. Qiao, Langmuir **24**, 11651 (2008).
[21] O. A. Basaran and D. W. DePaoli, Phys. Fluids **6**, 2923 (1994).
[22] J. S. Sharp, Soft Matter **8**, 399 (2012).
[23] V. R. Kern, J. B. Bostwick, and P. H. Steen, J. Fluid Mech. **923**, A5 (2021).
[24] Y. Xia and P. H. Steen, J. Fluid Mech., **841**, 767 (2018).
[25] Y. Xia and P. H. Steen, npj Microgravity **6**, 1 (2020).
[26] J. B. Bostwick and P. H. Steen, Annu. Rev. Fluid Mech. **47**, 539 (2015).
[27] M. Faraday, Phil. Trans. R. Soc. London **121**, 299 (1831).
[28] P. Brunet, J. Eggers, and R. D. Deegan, Phys. Rev. Lett. **99**, 144501 (2007).
[29] J. H. Snoeijer and B. Andreotti, Annu. Rev. Fluid Mech. **45**, 269 (2013).
[30] J. M. Ludwicki, V. R. Kern, J. McCraney, J. B. Bostwick, S. Daniel, and P. H. Steen, npj Microgravity **8**, 1 (2022).
[31] C. Jothi Prakash and R. Prasanth, J. Mater. Sci. **56**, 108 (2021).
[32] H. Li, A. Li, Z. Zhao, M. Li, and Y. Song, Small Struct. **1**, 2000028 (2020).
[33] Q. Li, D. Wu, and Z. Guo, Soft Matter **15**, 6803 (2019).
[34] J. Chi, X. Zhang, Y. Wang, C. Shao, L. Shang, and Y. Zhao, Mater. Horiz. **8**, 124 (2021).
[35] A. Kundan, J. L. Plawsky, P. C. Wayner, Jr., D. F. Chao, R. J. Sicker, B. J. Motil, T. Lorik, L. Chestney, J. Eustace, and J. Zoldak, Phys. Rev. Lett. **114**, 146105 (2015).
[36] D. Levine, B. Wise, R. Schulman, H. Gutierrez, D. Kirk, N. Turlesque, W. Tam, M. Bhatia, and D. Jaekle, J. Propul. Power **31**, 429 (2015).
[37] J. McCraney, M. Weislogel, and P. Steen, Fluids **5**, 207 (2020).
[38] J. McCraney, M. Weislogel, and P. Steen, npj Microgravity **7**, 1 (2021).

[39] M. Martin, J. Smolen, M. Weislogel, J. Thomas, and E. Peterson, in *Advancing, Static, and Receding Contact Angle Measurements for AF-M315E and Distilled Water on Different Materials and Surface Roughness, Tampa, FL* (2019).

[40] E. J. Hoffman, W. Ebert, M. Femiano, H. Freeman, C. Gay, C. Jones, P. Luers, and J. Palmer, Applied Physics Laboratory, Johns Hopkins University, Technical Report, 1999, https://spacese.spacegrant.org/Failure%20Reports/NEAR_Rendezvous_BurnMIB.pdf.